Journal of Geodesy
https://doi.org/10.1007/s00190-017-1089-8

ORIGINAL ARTICLE

The gravity field model IGGT_R1 based on the second invariant of the GOCE gravitational gradient tensor

Biao Lu[1,2,3] · Zhicai Luo[4,5] · Bo Zhong[1,6] · Hao Zhou[4] · Frank Flechtner[2,3] · Christoph Förste[2] · Franz Barthelmes[2] · Rui Zhou[7]

Received: 19 July 2016 / Accepted: 13 October 2017
© Springer-Verlag GmbH Germany, part of Springer Nature 2017

Abstract
Based on tensor theory, three invariants of the gravitational gradient tensor (IGGT) are independent of the gradiometer reference frame (GRF). Compared to traditional methods for calculation of gravity field models based on the gravity field and steady-state ocean circulation explorer (GOCE) data, which are affected by errors in the attitude indicator, using IGGT and least squares method avoids the problem of inaccurate rotation matrices. The IGGT approach as studied in this paper is a quadratic function of the gravity field model's spherical harmonic coefficients. The linearized observation equations for the least squares method are obtained using a Taylor expansion, and the weighting equation is derived using the law of error propagation. We also investigate the linearization errors using existing gravity field models and find that this error can be ignored since the used a-priori model EIGEN-5C is sufficiently accurate. One problem when using this approach is that it needs all six independent gravitational gradients (GGs), but the components V_{xy} and V_{yz} of GOCE are worse due to the non-sensitive axes of the GOCE gradiometer. Therefore, we use synthetic GGs for both inaccurate gravitational gradient components derived from the a-priori gravity field model EIGEN-5C. Another problem is that the GOCE GGs are measured in a band-limited manner. Therefore, a forward and backward finite impulse response band-pass filter is applied to the data, which can also eliminate filter caused phase change. The spherical cap regularization approach (SCRA) and the Kaula rule are then applied to solve the polar gap problem caused by GOCE's inclination of 96.7°. With the techniques described above, a degree/order 240 gravity field model called IGGT_R1 is computed. Since the synthetic components of V_{xy} and V_{yz} are not band-pass filtered, the signals outside the measurement bandwidth are replaced by the a-priori model EIGEN-5C. Therefore, this model is practically a combined gravity field model which contains GOCE GGs signals and long wavelength signals from the a-priori model EIGEN-5C. Finally, IGGT_R1's accuracy is evaluated by comparison with other gravity field models in terms of difference degree amplitudes, the geostrophic velocity in the Agulhas current area, gravity anomaly differences as well as by comparison to GNSS/leveling data.

Keywords Invariants of the gravitational gradient tensor · Least squares method · Linearization · Band-pass filter · GOCE

1 Introduction

The gravity field and steady-state ocean circulation explorer (GOCE) differs from previous Earth gravity satellite missions, e.g., challenging minisatellite payload (CHAMP) and gravity recovery and climate experiment (GRACE) as it can provide the much more detailed measurements of the GGs of Earth's gravity field. Calculation of gravity field models based on these measured GGs has become a very important research domain, and several methods for determination of gravity field models from GGs have been developed. The three main methods are the space-wise approach, the time-wise approach and the direct approach (Rummel and Colombo 1985; Rummel 1993; Klees et al. 2000; Pail and Plank 2002; Migliaccio et al. 2004, 2011; Bruinsma et al. 2010a, 2014; Pail et al. 2011; Yi 2012). The European Space Agency (ESA) has already distributed several gravity models constructed using these three methods through the International Centre for Global Earth Models (ICGEM) (Barthelmes 2009; Barthelmes and Förste 2011). The space-wise approach is based on least squares collocation and takes advantage of the spatial correlation of the gravitational field

✉ Bo Zhong
bzhong@sgg.whu.edu.cn

Extended author information available on the last page of the article

Published online: 29 November 2017

signal. The time-wise approach is based on a least squares method, but takes advantage of the time correlation of the gravitational field signal along the satellite's orbit. The direct approach is also based on a least squares method and builds observation equations and normal equations directly from in situ GOCE GGs. While processing the GGs for these methods, errors may be introduced when using the GOCE star tracker data to relate the azimuth of the GRF to other coordinate systems. Although the direct method uses GGs measured in the GRF to build the normal equation, the coefficients of every observation equation must be rotated from Earth-Centered Earth-Fixed coordinates to the GRF. Thus the inaccuracies in the transformation matrix cannot be avoided. Specifically, investigations by Pail and Plank (2002), Pail et al. (2005) and Yu and Zhao (2010) found that 1 arcsec attitude errors can lead the data processing accuracy to barely reach a relative magnitude of $10^{-6} - 10^{-7}$.

In view of this challenging problem, Rummel and Colombo (1985) began to investigate how to use the IGGT to build gravity field models. Holota (1989) discussed how to use the theory of boundary value problems for partial differential equations in satellite gradiometry. Then Sacerdote and Sansò (1989) analyzed the effects of orbit and attitude errors on GGs, and they found that using a reference gravity field including the J_2 term is preferable. At the same time, Vermeer (1990) built up three independent invariants and studied how the difference method for GGs could reduce the effects of the satellite's attitude and rotation. They also analyzed the spectrum relationship between the differencing method's result and the gravitational signal. More recently, Baur et al. (2008) expanded the invariant theory in detail from the invariant system and eigenspace. They parameterized the invariants and performed numerical simulations, but the parameterization in the spherical polar coordinate is complicated. Boundary value problems with a sphere approximation including a J_2 term are shown by Yu and Zhao (2010) and Yu and Wan (2013). Specifically, the gravity field models are built using spherical harmonic analysis according to the boundary value conditions. However, this requires gridding the GOCE gravitational gradient measurements and using spherical harmonic integral discretization which can introduce errors that are difficult to eliminate.

Based on these previous studies, we investigate how to use IGGT to directly determine gravity field models using a least squares method in this paper. We study the linearization of IGGT mathematically from the Taylor expansion. Furthermore, the Lagrange-type remainder or linearization error is investigated by existing, high accurate gravity field models to prove that it can be ignored when a-priori accurate gravity field model is chosen, e.g., EIGEN-5C (Förste et al. 2008). So it doesn't need iteratively calculations used by Baur et al. (2008) during numerical simulations to eliminate the linearization error which is time-consuming in the least squares method. As the non-uniform accuracy of GOCE GGs, the weighting formula of IGGT is derived by the law of error propagation. To deal with the inaccurate components V_{xy} and V_{yz}, we use synthetic GGs for both inaccurate gravitational gradient components derived from the a-priori gravity field model. As GOCE GGs are measured in a band-limited manner, filtering is necessary for different approaches. The Wiener filter along the orbit to reduce the highly time correlated noise of the gradiometer which is generally used for collocation procedure, e.g., the space-wise approach (Reguzzoni and Tselfes 2009). Autoregressive moving average filtering is applied to both the time-wise approach and the direct approach, but it is a kind of filtering of entire spectrum (full decorrelation) for the time-wise approach while filtering within the measurement bandwidth for the direct approach (Schuh 2003; Pail et al. 2011). We also applied a band-pass filter as the direct approach to suppress the signal outside the measurement bandwidth. This makes the result largely independent of the variability in the colored noise. Furthermore, we use a finite impulse response band-pass filter forward and backward to eliminate the filter caused phase change and the signals outside the measurement bandwidth are replaced by the a-priori model. In this way, it avoids to filter both sides of the observations and the columns of the design matrix during calculations like the time-wise approach and the direct approach. This kind of filtering and replacement method can be used both for spherical harmonic analysis and direct least squares method according to Wan et al. (2012). Therefore, the final gravity field model built in this paper is practically a combined one which is improved by GOCE GGs signals from the a-priori gravity field model. This is also one reason why we replace the inaccurate components V_{xy} and V_{yz} by the a-priori gravity field model. To verify our approach, we built a gravity field model called IGGT_R1 using GOCE GGs and we compared it with other relevant gravity field models and also evaluated it by using GNSS/leveling data.

2 The direct calculation model for IGGT

2.1 Tensor invariants method

According to the symmetric and trace-free characteristics of the gravitational gradient tensor, Γ, three invariants can be identified by:

$$\begin{cases} I_1 = \mathrm{tr}\,(\Gamma) = 0 \\ I_2 = \dfrac{1}{2}\,\mathrm{tr}\,(\Gamma)^2 = -\dfrac{1}{2}\left(V_{11}^2 + V_{22}^2 + V_{33}^2\right) \\ \qquad - V_{12}^2 - V_{13}^2 - V_{23}^2 \\ I_3 = \det \Gamma = V_{11}V_{22}V_{33} + 2V_{12}V_{13}V_{23} - V_{11}V_{23}^2 \\ \qquad - V_{22}V_{13}^2 - V_{33}V_{12}^2 \end{cases} \tag{1}$$

The first tensor invariant is the trace of the gravitational tensor and its application in geopotential recovery yields the trivial solution as shown by Baur et al. (2008). The second tensor invariant comprises all 6 independent gravitational gradient tensor components. Furthermore, it is a quadratic function of the spherical harmonic coefficients of the gravity field:

$$I_2 = I = -\frac{1}{2}\left(V_{xx}^2 + V_{yy}^2 + V_{zz}^2\right) - V_{xy}^2 - V_{xz}^2 - V_{yz}^2 \quad (2)$$

It has been shown in several theoretical studies (e.g., Baur et al. 2008; Rummel et al. 2011) that also the second as well as third invariant can be used to compute a global gravity model solution. Since the second invariant is easier to linearize than the third one, we focus on the second one here in this study.

2.2 Parameterization and linearization

The expression of the gravitational potential in terms of spherical harmonic series is given by [e.g., Heiskanen and Moritz (1967)]:

$$V(r,\vartheta,\lambda) = \frac{GM}{R}\sum_{n=0}^{N_{\max}}\left(\frac{R}{r}\right)^{n+1}\sum_{m=0}^{n}(\bar{C}_{nm}\cos m\lambda + \bar{S}_{nm}\sin m\lambda)\bar{P}_{nm}(\cos\vartheta) \quad (3)$$

where GM is the geocentric gravitational constant, R is Earth equatorial radius. In the following, the variable x represents the spherical harmonic coefficients as given in Eq. (4), the mathematical operator Sigma in Eq. (4) means the numbering scheme instead of the summation of elements as shown by Schuh (1996); the indexed gravity field model coefficients $\bar{C}_{nm}$ and $\bar{S}_{nm}$ are preferable for calculating the high-degree normal equation (e.g., Colombo 1981; Schuh 1996).

$$x = \{\bar{C}_{nm}, \bar{S}_{nm}\} \Rightarrow \left\{\sum_{n=2}^{n_{\max}}\bar{C}_{n0}, \sum_{m=1}^{n_{\max}}\left\{\sum_{n=\max(2,m)}^{n_{\max}}\bar{C}_{nm}, \sum_{n=\max(2,m)}^{n_{\max}}\bar{S}_{nm}\right\}\right\} \quad (4)$$

As the tensor invariant I in the GRF is same as in the local north-oriented frame (LNOF), we use it in the GRF directly, but linearize it in the LNOF. The tensor invariant I is a second-order function of the GGs in the LNOF, while the GGs in the LNOF are first-order functions of the spherical harmonic coefficients. Thus I is a quadratic function of the spherical harmonic coefficients. A Taylor expansion (Taylor 1717; Courant and John 2012) of I with the Lagrange form of the remainder is applied to generate Eq. (5):

$$I(x) - I(x_0) = \sum_{p=1}^{n=1}\frac{1}{p!}\left(\Delta x_1\frac{\partial}{\partial x_1} + \cdots + \Delta x_m\frac{\partial}{\partial x_m}\right)^p I(x)|_{x=x_0} + \frac{1}{(n+1)!}\left(\Delta x_1\frac{\partial}{\partial x_1} + \cdots + \Delta x_m\frac{\partial}{\partial x_m}\right)^{n+1} \times I(x)|_{x=x_0+\theta h} \quad (0<\theta<1) \quad (5)$$

where $x_1, x_2, ..., x_m$ are the spherical harmonic coefficients. The Taylor expansion of I exists since the first- and second-order partial derivatives of I with respect to x_i exist. Eq. (7) and Eq. (9) correspondingly yield the partial derivatives of I and the GGs with respect to x_i. In Eq. (5), n is equal to 1 as I contains only second-order partial derivatives of x_i, h is set to $x - x_0$ and θ is some real number between 0 and 1. For x_0, we choose EIGEN-5C as the a-priori gravity field model as it is of a relatively high accuracy and doesn't contain GOCE data. Next we analyze the Lagrange remainder, or the linearization error, using the existing, high accurate gravity field model EGM2008 (Pavlis et al. 2012) and another high accurate and GOCE containing gravity field model EIGEN-6C4 (Förste et al. 2015a) to calculate $I(x)$. The linearization error is defined by Eq. (6):

$$\begin{aligned}\mathrm{Error}_L &= I(x) - I(x_0) - \sum_{p=1}^{n=1}\frac{1}{p!}\left(\Delta x_1\frac{\partial}{\partial x_1} + \cdots + \Delta x_m\frac{\partial}{\partial x_m}\right)^p I(x)|_{x=x_0} \\ &= I(x) - I(x_0) - \left(\Delta x_1\frac{\partial I(x)|_{x=x_0}}{\partial x_1} + \cdots + \Delta x_m\frac{\partial I(x)|_{x=x_0}}{\partial x_m}\right)\end{aligned} \quad (6)$$

As shown in Eq. (6), the derivatives of I with respect to x_i should be determined before analyzing the linearization error using existing gravity field models. The purpose of the linearization is to determine the relationship between the IGGT and the gravity field model geopotential coefficients. The derivative of I with respect to x_i is based on Eq. (2) and given by Eq. (7):

$$\frac{\partial I}{\partial x_i} = -\left(V_{xx}\frac{\partial V_{xx}}{\partial x_i} + V_{yy}\frac{\partial V_{yy}}{\partial x_i} + V_{zz}\frac{\partial V_{zz}}{\partial x_i} + 2V_{xy}\frac{\partial V_{xy}}{\partial x_i} + 2V_{xz}\frac{\partial V_{xz}}{\partial x_i} + 2V_{yz}\frac{\partial V_{yz}}{\partial x_i}\right) \quad (7)$$

The transformation relationship of GGs between earth center spherical coordinates and LNOF is given by Eq. (8) as shown by Koop (1993) and is used to get the GGs' derivatives in the LNOF to geopotential coefficients of the gravity field model.

$$\begin{cases} V_{zz} = V_{rr} \quad V_{xx} = \frac{1}{r}V_r + \frac{1}{r^2}V_{\vartheta\vartheta} \\ V_{yy} = \frac{1}{r}V_r + \frac{1}{r^2\tan\vartheta}V_\vartheta + \frac{1}{r^2\sin^2\vartheta}V_{\lambda\lambda} \\ V_{xy} = \frac{1}{r^2\sin^2\vartheta}V_{\vartheta\lambda} - \frac{\cos\vartheta}{r^2\sin^2\vartheta}V_\lambda \\ V_{xz} = \frac{1}{r^2}V_\vartheta - \frac{1}{r}V_{r\vartheta} \quad V_{yz} = \frac{1}{r^2\sin\vartheta}V_\lambda - \frac{1}{r\sin\vartheta}V_{r\lambda} \end{cases} \quad (8)$$

The corresponding derivatives of the GGs with respect to the spherical harmonic coefficients are given in Eq. (9). The coefficients of the observation matrix are then obtained by substituting them into Eq. (7).

$$
\begin{cases}
\frac{\partial V_{zz}}{\partial \bar{C}_{nm}} = \frac{\mathrm{GMR}^n}{r^{n+3}}(n+1)(n+2)\bar{P}_{nm}(\cos\vartheta)\cos m\lambda \\
\frac{\partial V_{xx}}{\partial \bar{C}_{nm}} = \frac{\mathrm{GMR}^n}{r^{n+3}}\left(-(n+1)\bar{P}_{nm}(\cos\vartheta) + \frac{\partial^2 \bar{P}_{nm}(\cos\vartheta)}{\partial\vartheta}\right)\cos m\lambda \\
\frac{\partial V_{yy}}{\partial \bar{C}_{nm}} = \frac{\mathrm{GMR}^n}{r^{n+3}}\left(-(n+1)\bar{P}_{nm}(\cos\vartheta) + \frac{1}{\tan\vartheta}\frac{\partial \bar{P}_{nm}(\cos\vartheta)}{\partial\vartheta} - \frac{m^2}{\sin^2\vartheta}\bar{P}_{nm}(\cos\vartheta)\right)\cos m\lambda \\
\frac{\partial V_{xy}}{\partial \bar{C}_{nm}} = \frac{\mathrm{GMR}^n}{r^{n+3}}\left(-m\frac{1}{\sin\vartheta}\frac{\partial \bar{P}_{nm}(\cos\vartheta)}{\partial\vartheta} + m\frac{\cos\vartheta}{\sin^2\vartheta}\bar{P}_{nm}(\cos\vartheta)\right)\sin m\lambda \\
\frac{\partial V_{xz}}{\partial \bar{C}_{nm}} = \frac{\mathrm{GMR}^n}{r^{n+3}}(n+2)\frac{\partial \bar{P}_{nm}(\cos\vartheta)}{\partial\vartheta}\cos m\lambda \\
\frac{\partial V_{yz}}{\partial \bar{C}_{nm}} = \frac{\mathrm{GMR}^n}{r^{n+3}}\frac{1}{\sin\vartheta}\left(-m(n+2)\bar{P}_{nm}(\cos\vartheta)\right)\sin m\lambda \\
\frac{\partial V_{zz}}{\partial \bar{S}_{nm}} = \frac{\mathrm{GMR}^n}{r^{n+3}}(n+1)(n+2)\bar{P}_{nm}(\cos\vartheta)\sin m\lambda \\
\frac{\partial V_{xx}}{\partial \bar{S}_{nm}} = \frac{\mathrm{GMR}^n}{r^{n+3}}\left(-(n+1)\bar{P}_{nm}(\cos\vartheta) + \frac{\partial^2 \bar{P}_{nm}(\cos\vartheta)}{\partial\vartheta}\right)\sin m\lambda \\
\frac{\partial V_{yy}}{\partial \bar{S}_{nm}} = \frac{\mathrm{GMR}^n}{r^{n+3}}\left(-(n+1)\bar{P}_{nm}(\cos\vartheta) + \frac{1}{\tan\vartheta}\frac{\partial \bar{P}_{nm}(\cos\vartheta)}{\partial\vartheta} - \frac{m^2}{\sin^2\vartheta}\bar{P}_{nm}(\cos\vartheta)\right)\sin m\lambda \\
\frac{\partial V_{xy}}{\partial \bar{S}_{nm}} = \frac{\mathrm{GMR}^n}{r^{n+3}}\left(m\frac{1}{\sin\vartheta}\frac{\partial \bar{P}_{nm}(\cos\vartheta)}{\partial\vartheta} - m\frac{\cos\vartheta}{\sin^2\vartheta}\bar{P}_{nm}(\cos\vartheta)\right)\cos m\lambda \\
\frac{\partial V_{xz}}{\partial \bar{S}_{nm}} = \frac{\mathrm{GMR}^n}{r^{n+3}}(n+2)\frac{\partial \bar{P}_{nm}(\cos\vartheta)}{\partial\vartheta}\sin m\lambda \\
\frac{\partial V_{yz}}{\partial \bar{S}_{nm}} = \frac{\mathrm{GMR}^n}{r^{n+3}}\frac{1}{\sin\vartheta}\left(m(n+2)\bar{P}_{nm}(\cos\vartheta)\right)\cos m\lambda
\end{cases}
\tag{9}
$$

In next step, the linearization error is investigated using existing gravity field models along with GOCE track data which will be presented in Sect. 4.

2.3 Determine the weighting formula

After linearization, which gives the observation matrix coefficients, the IGGT weighting formula is deduced by differentiating Eq. (2) to get Eq. (10):

$$
\begin{aligned}
dI = &-(V_{xx}dv_{xx} + V_{yy}dv_{yy} + V_{zz}dv_{zz}) \\
&-2(V_{xy}dv_{xy} + V_{yz}dv_{yz} + V_{xz}dv_{xz})
\end{aligned}
\tag{10}
$$

Using the adjusted law of measurement error propagation (Teunissen 2000), the variance of the IGGT is given by Eq. (11):

$$
\begin{aligned}
D(I) = K D_{GGs} K^T = &V_{xx}^2\sigma_{xx}^2 + V_{yy}^2\sigma_{yy}^2 + V_{zz}^2\sigma_{zz}^2 \\
&+4V_{xy}^2\sigma_{xy}^2 + 4V_{yz}^2\sigma_{yz}^2 + 4V_{xz}^2\sigma_{xz}^2
\end{aligned}
\tag{11}
$$

Since the V_{xy} and V_{yz} values for GOCE are degraded by a factor of 100–1000 (Catastini et al. 2006), they are replaced in our study by synthetic values based on the a-priori model (c.f. Sect. 3 for details). Therefore, the terms $4V_{yz}^2\sigma_{yz}^2$ and $4V_{xy}^2\sigma_{xy}^2$ in Eq. (11) are not included for the calculation of $D(I)$. Finally, Eq. (12) gives the single weighting of the gravitational tensor invariant:

$$
P_i = 1/D(I_i) \tag{12}
$$

2.4 Regularization

Due to the problem of the polar gap in the GOCE data, the normal equation matrix based on the GOCE GGs is ill-conditioned and must be regularized. We apply the SCRA as proposed by Metzler and Pail (2005) to the GOCE gravitational gradient normal equation from degree/order 2–150. Since the parameter vector x contains different coefficients than the a-priori model EIGEN-5C, we choose the stabilizing function $g_0 = 0$ [according to formula 27 in Metzler and Pail (2005)]. Furthermore, for degree/order 150 and higher, Kaula's rule of thumb (Rapp 1973; Reigber 1989) is applied to the normal equation because for this degree range the low-order coefficients as well as all other short wavelength spherical harmonic coefficients are disturbed by the polar gap and the increasing sensitivity of the GOCE gradiometer. This can be seen in Fig. 4a. The optimal SCRA and Kaula rule parameters are empirically determined by comparing model-derived geoid heights with GNSS/leveling data rather than with RMS geoid errors, as shown by Metzler and Pail (2005). We use this approach because the real gravity field, which is required to calculate the RMS geoid error, is unknown and

this approach is best suited for simulations. The high accuracy of the GNSS/leveling data and their wide distribution over several different countries and continents (see Table 2) make them best suitable for evaluation of our method.

3 Processing the gravitational gradients

3.1 Preprocessing

We use the components V_{xx}, V_{yy}, V_{zz} and V_{xz} of the GOCE GGs in the GRF taken from the Level2 product EGG_NOM_2 (ESA) which also contains the GRF to Inertial Reference Frame (IRF) attitude quaternions. For consistency with ESA's first generation gravity field models, we use data from November 01, 2009 to January 11, 2010. Furthermore, we use the GOCE orbit position given in the Earth-fixed Reference Frame (ERF) from the GOCE orbit product SST_PSO_2 which also includes the ERF to IRF quaternions. To deal with the two remaining but worse components of the GOCE GGs, a replacement strategy is used as described for the generation of ESA's GOCE product EGG_TRF_2 (Gruber et al. 2010). Here, the degraded components V_{xy} and V_{yz} of the GOCE GGs had been replaced by those computed from GOCE quick-look solution. But having in mind that the GOCE quick-look gravity field solutions are not computable satisfactory (Mayrhofer et al. 2010), we use reference GGs from the a-priori gravity field model EIGEN-5C to replace the worse components V_{xy} and V_{yz}. The reference U_{GRF} value for the GGs should first be calculated using EIGEN-5C in the LNOF (U_{LNOF}) and then transformed to the GRF (e.g., Fuchs and Bouman 2011; Bouman et al. 2011):

$$U_{\mathrm{GRF}} = \left(R^{\mathrm{IRF}}_{\mathrm{GRF}} R^{\mathrm{ERF}}_{\mathrm{IRF}} R^{\mathrm{LNOF}}_{\mathrm{ERF}}\right) U_{\mathrm{LNOF}} \left(R^{\mathrm{IRF}}_{\mathrm{GRF}} R^{\mathrm{ERF}}_{\mathrm{IRF}} R^{\mathrm{LNOF}}_{\mathrm{ERF}}\right)^{T} \tag{13}$$

where $R^{\mathrm{IRF}}_{\mathrm{GRF}}$ represents the transformation matrix to convert from the IRF to the GRF and $R^{\mathrm{ERF}}_{\mathrm{IRF}}$ is the transformation matrix to convert from ERF to IRF (which is taken from the quaternions in SST_PSO_2). The transformation matrix from LNOF to ERF is given by $R^{\mathrm{LNOF}}_{\mathrm{ERF}}$ and is taken from Eq. (14). Here, the latitude and longitude, λ and φ as well as the colatitude, $\vartheta = \pi/2 - \varphi$, can be calculated from the SST_PSO_2 orbit coordinates. The right side of U_{LNOF} in Eq. (13) is the transpose of $R^{\mathrm{IRF}}_{\mathrm{GRF}} R^{\mathrm{ERF}}_{\mathrm{IRF}} R^{\mathrm{LNOF}}_{\mathrm{ERF}}$.

$$R^{\mathrm{LNOF}}_{\mathrm{ERF}} = \begin{bmatrix} -\cos\lambda\cos\vartheta & \sin\lambda & \cos\lambda\sin\vartheta \\ -\sin\lambda\cos\vartheta & -\cos\lambda & \sin\lambda\sin\vartheta \\ \sin\vartheta & 0 & \cos\vartheta \end{bmatrix} \tag{14}$$

3.2 Filtering processing

After the reference GGs are calculated, the residuals of the used four GOCE gravity gradient components are obtained by subtracting the reference GGs from the measured GOCE GGs. These must then be filtered because the GOCE GGs are band-limited measurements. A forward and backward finite impulse response band-pass filter is used to account for the band-limited measurements according to Wan et al. (2012). This approach can also eliminate phase change after filtering. As Fig. 1 shows, the filter is of 1000th order with a band-pass frequency of 8.3–125 mHz. This band-pass frequency ensures that the results are as far as possible independent of the temporal variations in the colored noise (Bruinsma et al. 2014). The synthetic gravity gradient components V_{xy} and V_{yz} are not filtered and are taken as error-free observations. Figure 2 shows a power spectrum diagram of the filtering results; the spectral densities (SDs) for the gradient signal computed with the gravity field model are shown in red, the SDs for the GOCE gradient signal are shown in blue, and the difference in SDs between the gravity field model and the measured gradients, filtered to the band-pass frequency, is shown in green. The black line indicates the lower end of the specified band-pass frequency (8.3 mHz), and the cyan line indicates the upper end (125 mHz). The power spectrum of the signal in the filter band-pass remains almost the same, while the power spectrum of the signal outside the pass-band is obviously decreased, representing a very small proportion of the total signal. This demonstrates the effectiveness of the filtering process. After filtering, we use the four accurate gravity gradient disturbance components, and their corresponding reference GGs, along with two other reference GGs to finally construct the gravitational gradient tensor as shown in Eq. (2).

4 Development of IGGT_R1

After determining the mathematic model and the stochastic model, we use GOCE GGs to build the gravity field model IGGT_R1. The main flowchart is shown in Fig. 3: The input data and the filtering method are described in Sect. 3; the main methodology to use GOCE IGGT to build gravity field models by least squares method is mentioned in Sect. 2. The rest detailed information of development of IGGT_R1 are given out as follows: EIGEN-5C is chosen as the a-priori gravity field model which is used to calculate $I(x_0)$ for linearization error analysis. As mentioned before, EGM2008 and EIGEN-6C4 are used to calculate $I(x)$ to analyze the linearization error according to Eq. 6. The positions are from one day's GOCE track data of 1 sec sampling rate, and the maximum degree/order of the gravity field models is set to 240. The linearization error statistics are given in Table 1.

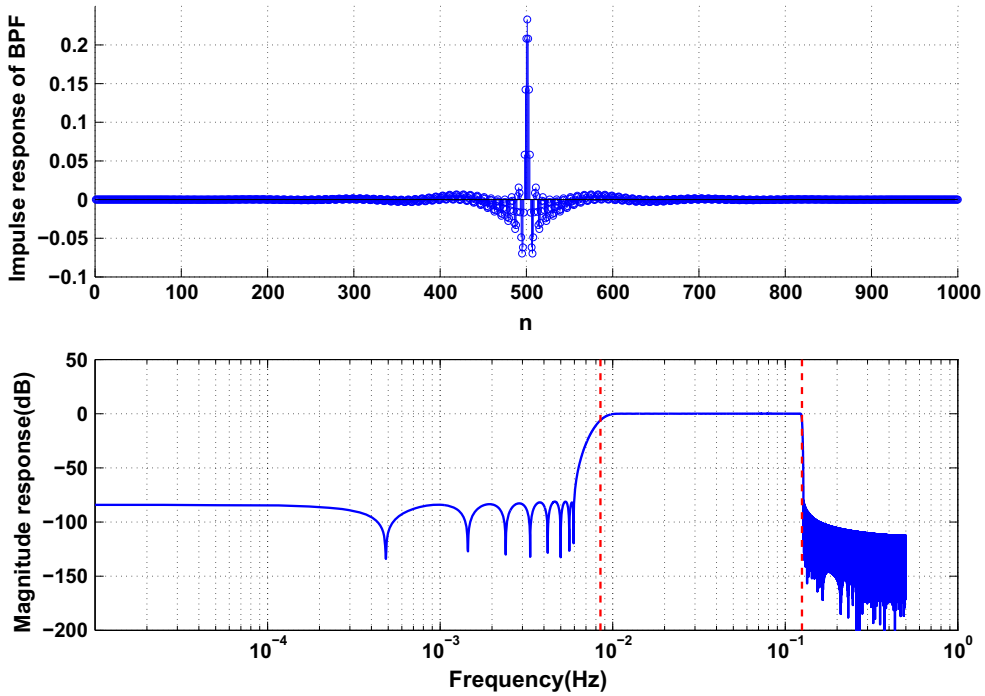

Fig. 1 Finite impulse response band-pass filter. The up half figure is the impulse response of the band-pass filter; The other half one is the magnitude response of the band-pass filter (unit: dB)

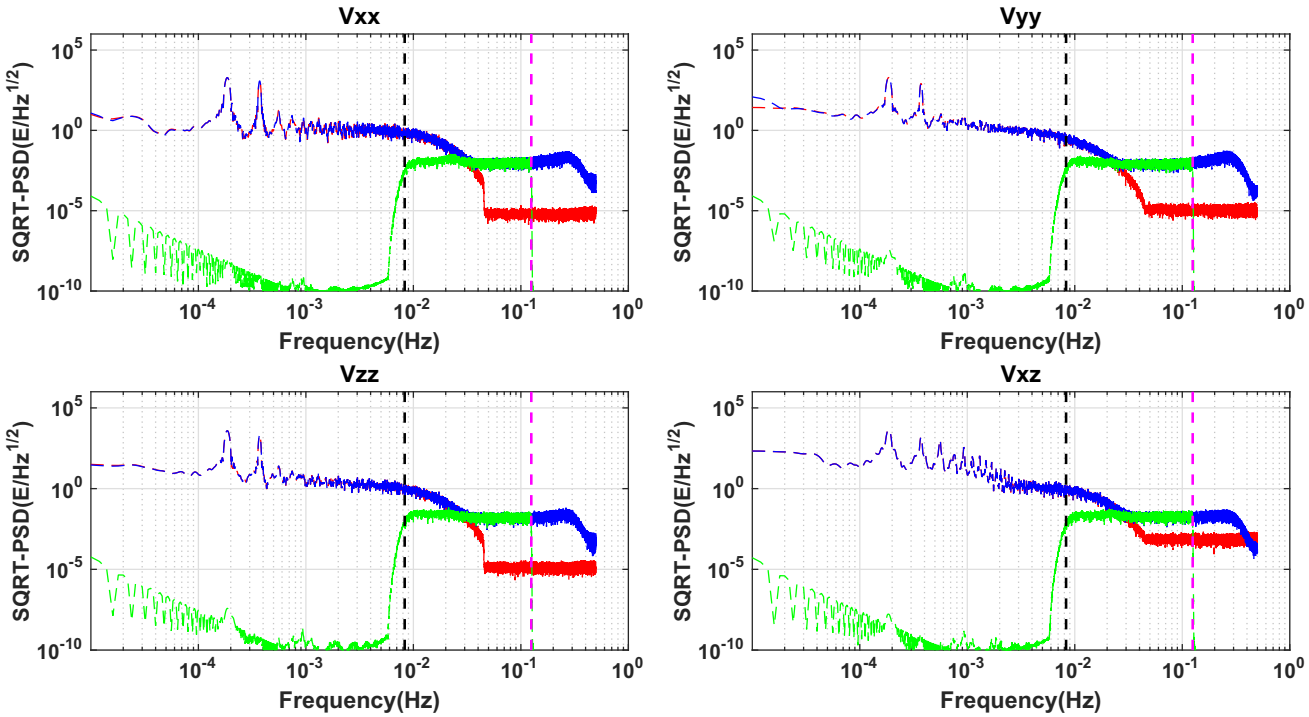

Fig. 2 Spectral densities for V_{xx}, V_{yy}, V_{zz} and V_{xz} for GRF (unit: $\mathrm{E}/\sqrt{\mathrm{Hz}}$). In red the spectral densities for the gradient signal computed with gravity field model, in blue the SDs for GOCE gradient signal, in green the SDs of the difference between gravity field model and measured gradients filtered to the band-pass frequency

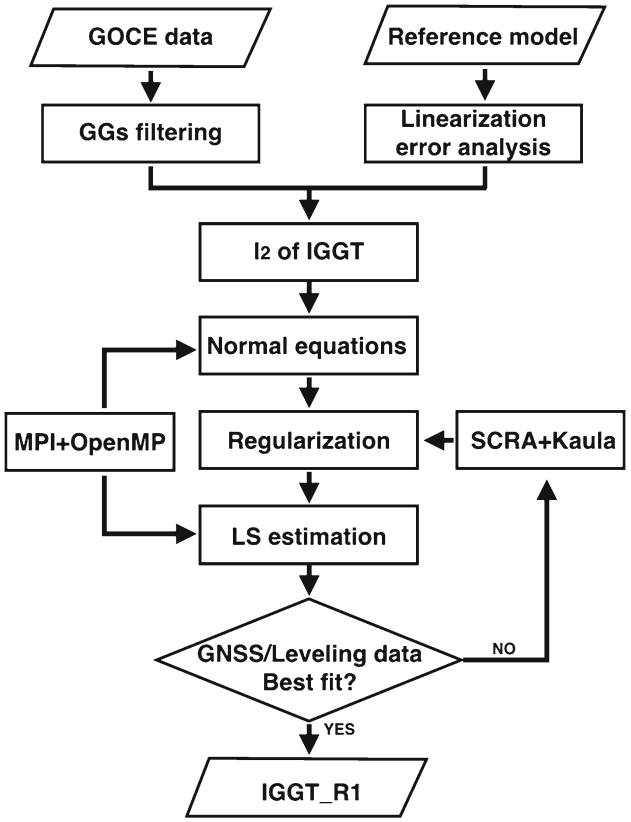

Fig. 3 Flowchart of the development of IGGT_R1. The LS estimation in the flowchart means least square estimation

Here, the relative linearization error (RLE) is defined using Eq. (15):

$$\mathrm{RLE} = \frac{1}{N}\sum_{i=1}^{N}\left|\frac{\mathrm{Error}_{Li}}{I(x)_i}\right| \tag{15}$$

where N is the number of GOCE track data points. The relative linearization error is only about 0.00071% for the EGM2008 model and 0.00042% for the EIGEN-6C4 model. Using Eq. (10) and considering that the real accuracy of the GOCE GGs is of 2–4 mE (Bouman and Fuchs 2012), the maximum absolute linearization error is approximately 10^{-21} s^{-4} and σ_I is $\sim 10^{-17} - 10^{-16}$ s^{-4}. This means the linearization error can be neglected in this study.

After studying the linearization error, one important step in the flowchart of the development of IGGT_R1 is about regularization which is already explained in Sect. 2.4. The results by compared with coefficients of EGM2008 are shown in Fig. 4: The SCRA and Kaula rule are effective by comparing these two sub-figures before and after regularization. It can be seen from the post-regularization spectrum errors in Fig. 4b, and the low-order coefficients and some short wavelength spherical harmonic coefficients are improved after regularization.

Table 1 Statistics of the linearization error of the a-priori gravity field model EIGEN-5C according to EGM2008 and the GOCE containing gravity field model EIGEN-6C4 as "true" models (unit: s^{-4})

	EGM2008	EIGEN-6C4
Min	1.148699814359e−27	2.308982773258e−27
Max	2.167034978949e−21	7.978301266328e−22
Mean	2.090407160224e−23	1.497315373357e−23
STD	8.934785293679e−23	4.507380756543e−23
RLE	0.000711476171%	0.000423359387%

In the calculating process of building up gravity field models, especially dealing with a large number of satellite gravity measurement date sets by least square method, it needs to undertake large-scale numerical calculation. Aiming at this problem, we combine message passing interface (MPI) and open multiprocessing (OpenMP) technology which also takes advantage of the symmetrical feature of normal equation matrix during the calculation. In this way, it can greatly accelerate the computation speed and improve the computational efficiency. The characteristic of MPI is processing level parallel granularity and memory data are distributed storage, so it can effectively decompose the program on different nodes at the same time to shorten running time while the characteristic of OpenMP is thread level little granularity and memory data are shared storage, especially for calculating multiplication of small block matrix on the same node, so it can make full use of CPUs on single node to speed up the calculation process (e.g., Pacheco 1997; Gropp et al. 1999; Chandra 2001; Chapman et al. 2008).

5 Numerical results and analysis

To evaluate the spectral behavior, we computed difference degree amplitudes for IGGT_R1 to EGM2008 and compared them to those for the gravity field models GO_CONS_GCF_2_TIM_R1 (TIM_R1), GO_CONS_GCF_2_SPW_R1 (SPW_R1) and GO_CONS_GCF_2_DIR_R2 (DIR_R2). TIM_R1 and SPW_R1 are part of ESA's first release of GOCE gravity field models (Pail et al. 2011) while DIR_R2 is part of ESA's second release of GOCE gravity field models (Bruinsma et al. 2010b). We compare IGGT_R1 with TIM_R1 and SPW_R1 as the data period for the GOCE GGs is the same. But we choose DIR_R2 instead of GO_CONS_GCF_2_DIR_R1 (DIR_R1) which belongs the ESA's first release of GOCE gravity field models since the high-degree parts of the model DIR_R1 are strongly constrained by regularization using a combined gravity field model containing terrestrial data (Pail et al. 2011). Figure 5 shows the obtained difference degree amplitudes. In the low-degree part (degree is less than 70), IGGT_R1 is closer to

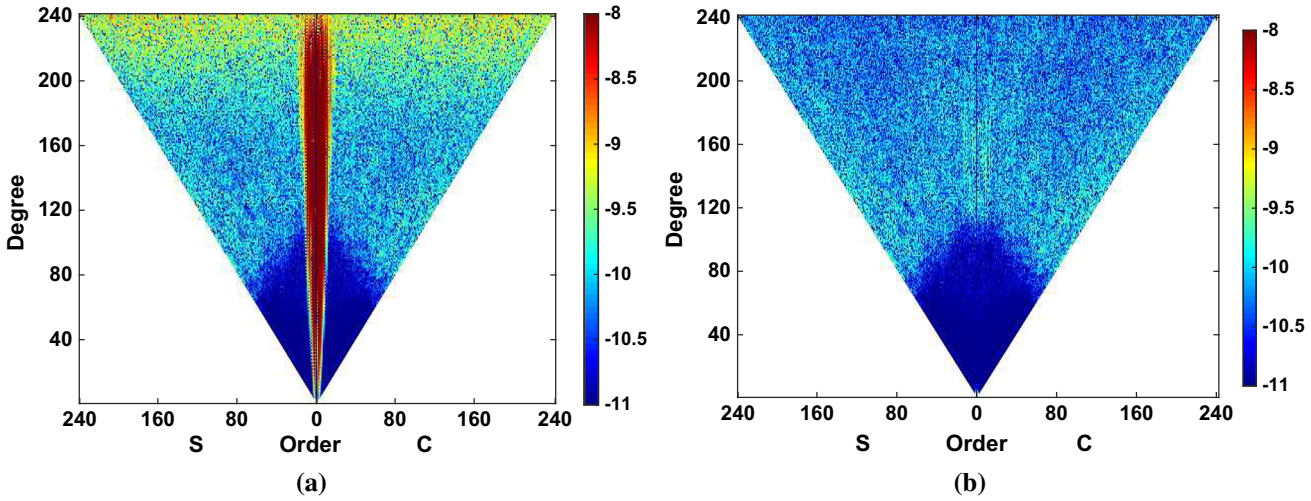

Fig. 4 Coefficient differences between IGGT_R1 and EGM2008 before regularization (**a**), after regularization (**b**), provided as absolute values in logarithmic scale ($\log_{10}$)

EGM2008 and consequently more accurate than TIM_R1, SPW_R1 and DIR_R2. This is because the SCRA is used for the low-degree part of IGGT_R1, and the GGs signal is replaced by the a-priori model EIGEN-5C outside the measurement bandwidth. It means that the low-degree part more closely matches the EIGEN-5C model (the blue line in the figure). From degree 75 to ∼ 175, IGGT_R1 is almost the same as TIM_R1, SPW_R1 and DIR_R2. This means that the contribution from the GOCE GGs to these gravity field models is basically the same at this degree range. In the high-end part (above degree 175), the difference degree amplitudes of IGGT_R1 are slightly lower than those of TIM_R1, SPW_R1 and DIR_R2. The main reason for this might be that the different regularization methods and parameters influence this part. When comparing IGGT_R1 with the a-priori model EIGEN-5C from degree 100 to 210, they are indistinguishable here, but the difference degree amplitudes of IGGT_R1 are slightly smaller than those for EIGEN-5C. This means that IGGT_R1 might be more precise than EIGEN-5C in this region thanks to the GOCEGGs.

Figure 6 shows gravity anomaly differences between IGGT_R1 and EIGEN-5C. The large differences in Antarctica, South America, Africa, west China and Indonesia represent improvements due to the GOCE GGs. In other places like north America and Australia, EIGEN-5C already contains good ground gravimetry data. Figure 7 shows a histogram of the gravity anomaly differences between IGGT_R1 and EIGEN-5C. The minimum, maximum, mean and standard deviation of the gravity anomaly differences are −41.609, 49.791, −0.009 and 4.787 mGal, respectively.

In addition to our comparison with other global gravity field models, we check IGGT_R1 also using GNSS/leveling data as independent data sets. Table 2 gives the RMS of the differences between GNSS/leveling data and the model-

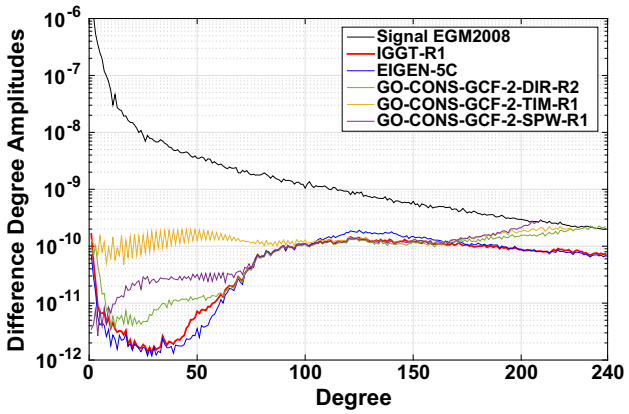

Fig. 5 Difference degree amplitudes (unitless) of several gravity field models w.r.t. EGM2008. The degree amplitudes of the EGM2008 model (black) are shown for reference

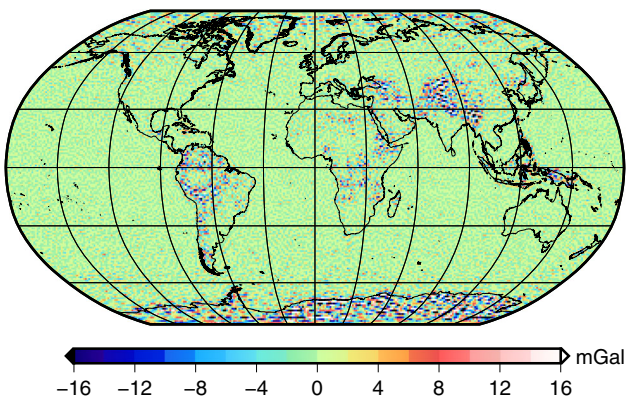

Fig. 6 Gravity anomaly differences (unit: mGal) between IGGT_R1 and EIGEN-5C at degree/order 240

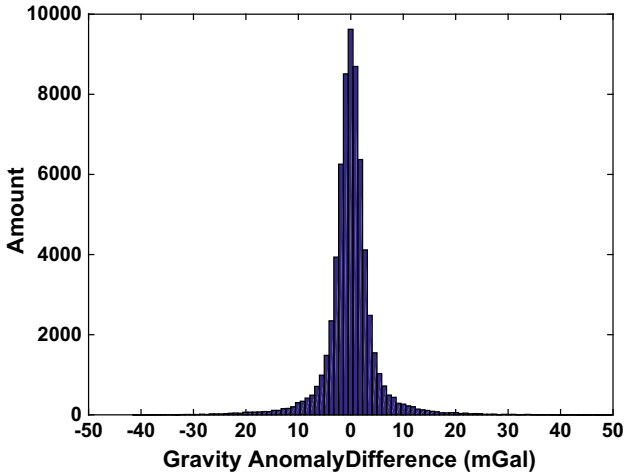

Fig. 7 Histogram of the gravity anomaly differences from Fig. 6 (unit: mGal). min/max/mean/STD are −41.609/49.791/−0.009/4.787 mGal

derived geoid heights. In the first column of the table, SPW_R1, TIM_R1, DIR_R1 and DIR_R2 indicate the gravity field models mentioned before. From the table, the results of DIR_R1 are better than those of DIR_R2. This should be caused by the matter of fact that DIR_R1 has been regularized by using a combined gravity field model which contains terrestrial data. We also see that IGGT_R1 gives better results than SPW_R1 and TIM_R1. This should be caused by the impact of the a-priori model EIGEN-5C during the replacement procedure for the degraded components V_{xy} and V_{yz} of the GOCE GGs as mentioned above. That means IGGT_R1 has not only contributions from the GOCE GGs but contains also gravity field information from the a-priori gravity field model EIGEN-5C. Thus the results of the GNSS/leveling check are relatively better. In comparison with DIR_R1 and DIR_R2, our model performs best in Germany and Japan with RMS values of 0.304 and 0.545 m. In other places, IGGT_R1, DIR_R1 and DIR_R2 have similar RMS values. By comparing with the a-priori gravity field model, the overall accuracy of IGGT_R1 is better or equal than EIGEN-5C. Specifically, the difference of the GNSS/leveling performance between IGGT_R1 and EIGEN-5C is not very large for Germany, USA and Canada. The reason here may be that the a-priori gravity field model EIGEN-5C is already very accurate in these regions due to precise ground gravimetry data. The RMS difference between IGGT_R1's geoid heights and GNSS/leveling data in Europe, Australia, Japan are improved by 1.5, 0.7 and 0.5 cm, respectively, due to the GOCE GGs. But for Brazil and China where EIGEN-5C has almost no contributions from terrestrial data we see a significant improvement by 6.7 and 4.1 cm due to the contribution of the GOCE GGs. It is also certified that the large gravity anomaly differences in South America and west China represent improvements due to the GOCE GGs as mentioned before. Furthermore, to examine the influence of different a-priori gravity field models to the approach in this paper, we also choose EGM2008 as the a-priori gravity field

Table 2 The RMS difference between GNSS/leveling data (number of points in brackets) and model-derived geoid heights (unit: m)

	Germany (675)	USA (6169)	Canada (1930)	Europe (1234)	Australia (201)	Japan (816)	Brazil (672)	China (990)
IGGT_R1	0.304	0.454	0.352	0.459	0.355	0.545	0.434	0.582
EIGEN-5C	0.303	0.456	0.353	0.474	0.362	0.550	0.501	0.623
IGGT_R1*	0.309	0.448	0.350	0.453	0.350	0.542	0.421	0.549
EGM2008	0.306	0.447	0.344	0.455	0.356	0.536	0.457	0.579
EIGEN-6S4v2	0.308	0.447	0.345	0.452	0.355	0.542	0.419	0.540
SPW_R1	0.331	0.470	0.399	0.495	0.383	0.569	0.447	0.589
TIM_R1	0.337	0.460	0.376	0.485	0.379	0.575	0.433	0.577
DIR_R1	0.308	0.446	0.349	0.458	0.354	0.546	0.417	0.552
DIR_R2	0.322	0.450	0.356	0.456	0.370	0.555	0.422	0.572

All models are taken to degree/order 210 which is the maximum degree of SPW_R1. IGGT_R1* is a gravity field model calculated as same as IGGT_R1 except that its a-priori model is EGM2008

Sources/references for the used GNSS/Leveling data:

USA: Milbert (1998)

Canada: M. Vronneau, personal communication 2003, Natural Resources Canada

Europe/Germany: Ihde et al. (2002)

Australia: G. Johnston, Geoscience Australia and W. Featherstone, Curtin University of Technology, personal communication 2007

Japan: Tokuro Kodama, Geospatial Information Authority of Japan, personal communication (2013)

Brazil: Denizar Blitzkow and Ana Cristina Oliveira Cancoro de Matos, Centro de Estudos de Geodesia (CENEGEO), personal communication, the data belongs to the Brazilian Institute of Geography and Statistics (IBGE)

China: National GNSS/leveling A/B: Zhang et al. (2009) and Li et al. (2014)

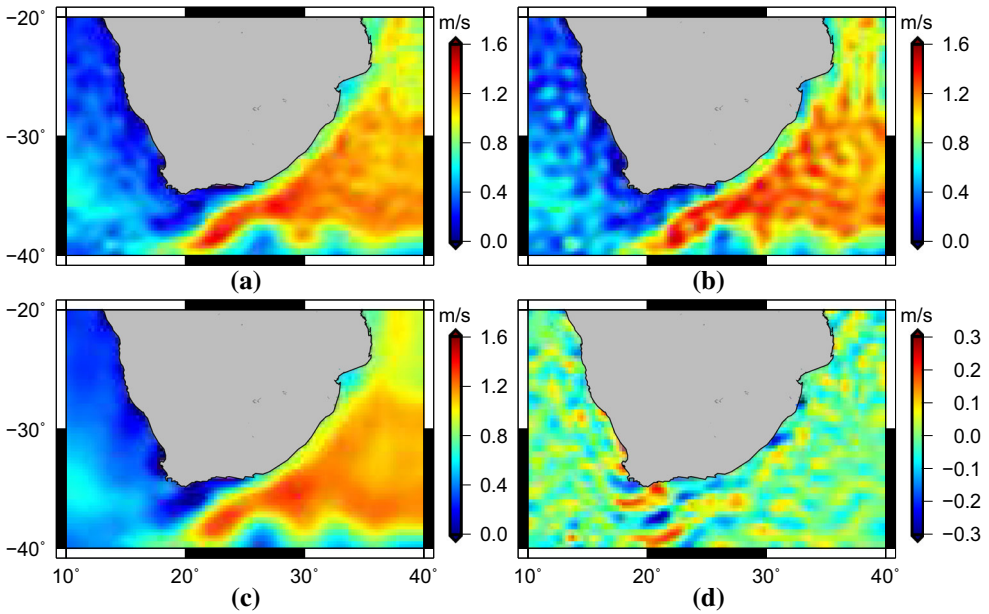

Fig. 8 Geostrophic velocity speed (unit: ms^{-1}) in the Agulhas current area at a resolution of about 27 km from **a** IGGT_R1, **b** TIM_R1 and **c** EIGEN-5C. **d** Shows the difference in geostrophic velocity speed between IGGT_R1 and EIGEN-5C

model to build a gravity field model named IGGT_R1*. The GNSS/leveling checking results are also shown in Table 2: IGGT_R1* is better than IGGT_R1 and reaches the accuracy of the latest satellite-only gravity field model EIGEN-6S4v2 (Förste et al. 2015b); The overall improvement of IGGT_R1* to EGM2008 is in Brazil and China by 3.6 and 3.0 cm. The reason here may be that the accuracy of EGM2008 is higher than EIGEN-5C and is already very good at some places where exist precise terrestrial data. But GOCE GGs have contributions in the other places.

Finally, we apply an oceanographic evaluation on IGGT_R1. Figure 8 shows the geostrophic velocity speed in the Agulhas current area at a resolution of about 27 km. Geostrophic velocity speed is derived from the ocean's mean dynamic topography (MDT), as described by Knudsen and Benveniste (2011) and Knudsen et al. (2011). A remove–restore technique is used to compute the combined MDT, which contains both the low-frequency signal of satellite-only MDT and the high-frequency signal from the a-priori MDT (MDT_DTU_10_2M.nc). MDT_DTU_10_2M.nc is produced by the Danish National Space Center and it includes TOPEX Ellipsoid and Mean-Tide system metadata. As can be seen from Fig. 8, the geostrophic velocity speed from IGGT_R1 is not as smooth as that from EIGEN-5C. Panel d of Fig. 8 shows the difference between these two models. The minimum, maximum, mean and RMS of the difference between the models are −0.310, 0.219, −0.0068, and 0.0589 ms^{-1}, respectively. These differences might be due to the GOCE GGs, but this cannot be confirmed without real drifter velocity measurements. The geostrophic velocity speed from TIM_R1 is a little more discrepant with EIGEN-5C. The main reason for this might be that the low-degree coefficients of TIM_R1 are not very accurate, as shown in Fig. 5.

6 Discussion and conclusions

The gravity field model IGGT_R1 has been generated using the GOCE IGGT by least squares method as described in this article. Due to the special characteristics of IGGT, this model avoids errors introduced by inaccurate measurement of the satellite's attitude during the traditional coordinate transformations. Additionally, according to the principle of least squares, the direct solution method is theoretically strict and there are no grid or integral discretization errors introduced in the harmonic analysis. The linearization error can be neglected if the a-priori gravity field model is relatively accurate. In such a case the corresponding linearization error is smaller than the accuracy of the GOCE GGs. Using the SCRA in combination with the Kaula rule is an effective way to solve the ill-conditioned problem of the normal equation which primarily helps to improve the low-order coefficients. From numerical analyses, we show that the precision of the obtained gravity anomaly values over Antarctica, South America, Africa, west China and Indonesia are improved due to the GOCE GGs. The RMS difference between GNSS/leveling data and the model-derived geoid heights shows that IGGT_R1 is more precise than SPW_R1 and TIM_R1, and it performs similarly to DIR_R1 and

DIR_R2. In comparison with the a-priori gravity field model EIGEN-5C, the whole accuracy of IGGT_R1 is improved according to the GNSS/leveling checking results. This represents the contribution of the GOCE GGs, especially in Brazil and China. According to geostrophic velocity speeds in the Agulhas current area, IGGT_R1, which yields more details because of the GOCE GGs, might be an improvement over EIGEN-5C. Considering time-consuming of calculation by the least squares method, IGGT_R1 contains the same GOCE GGs as ESA's first released gravity field models. In the future, all the GGs data of GOCE mission may be contained to calculate a more precise gravity field model. Our conclusion is that high precision gravity field models can be obtained using the approach as outlined in this paper. This provides a new direction for building gravity field models from the GOCE GGs as well as from future satellite GGs.

Acknowledgements Thanks for the constructive comments and beneficial suggestions from the anonymous reviewers and editors, which help us a lot for improving this manuscript. We also would like to express appreciation to Dr. X.Y. Wan of Qian Xuesen Laboratory of Space Technology (QLST), Dr. O. Abrykosov of German Research Centre for Geosciences (GFZ) and Dr. J. Bouman of German Geodetic Research Institute (DGFI) for their kind help and discussions. Thanks for the European Space Agency for providing the GOCE data. This study is supported by the Chinese Scholarship Council (No. 201506270158), the Natural Science Foundation of China (Nos. 41104014, 41131067, 41374023, 41474019 and 41504013) and the Key Laboratory of Geospace Environment and Geodesy, Ministry Education, Wuhan University (No. 16-02-07).

References

Barthelmes F (2009) Calculation service ICGEM. http://icgem.gfz-potsdam.de

Barthelmes F, Förste C (2011) The ICGEM-format. Potsdam: GFZ German Research Centre for Geosciences, Department 1

Baur O, Sneeuw N, Grafarend EW (2008) Methodology and use of tensor invariants for satellite gravity gradiometry. J Geod 82(4–5):279–293

Bouman J, Fuchs MJ (2012) GOCE gravity gradients versus global gravity field models. Geophys J Int 189(2):846–850

Bouman J, Fiorot S, Fuchs M, Gruber T, Schrama E, Tscherning C, Veicherts M, Visser P (2011) GOCE gravitational gradients along the orbit. J Geod 85(11):791–805

Bruinsma S, Marty J, Balmino G, Biancale R, Foerste C, Abrikosov O, Neumayer H (2010a) GOCE gravity field recovery by means of the direct numerical method. In: Paper presented at the ESA living planet symposium, European Space Agency, Bergen Norway, June pp 28–2

Bruinsma SL, Förste C, Abrikosov O, Lemoine JM, Marty JC (2010b) ESAs GOCE gravity field model from the direct approach release 2. ICGEM data base at GFZ Potsdam. http://icgem.gfz-potsdam.de/icgem/icgem.html

Bruinsma SL, Förste C, Abrikosov O, Lemoine JM, Marty JC, Mulet S, Rio MH, Bonvalot S (2014) ESA's satellite-only gravity field model via the direct approach based on all GOCE data. Geophys Res Lett 41(21):7508–7514

Catastini G, Cesare S, De Sanctis S, Dumontel M, Parisch M, Sechi G (2006) Predictions of the GOCE in-flight performances with the end-to-end system simulator. In: Proceedings of the 3rd international GOCE user workshop, pp 6–8

Chandra R (2001) Parallel programming in OpenMP. Morgan kaufmann, Burlington

Chapman B, Jost G, Van Der Pas R (2008) Using OpenMP: portable shared memory parallel programming, vol 10. MIT Press, Cambridge

Colombo OL (1981) Numerical methods for harmonic analysis on the sphere. Technicl report, DTIC Document

Courant R, John F (2012) Introduction to calculus and analysis, vol 1. Springer, Berlin

Förste C, Flechtner F, Schmidt R, Stubenvoll R, Rothacher M, Kusche J, Neumayer KH, Biancale R, Lemoine JM, Barthelmes F, Bruinsma J, König R, Meyer U (2008) EIGEN-GL05C-A new global combined high-resolution GRACE-based gravity field model of the GFZ-GRGS cooperation. In: Geophysical research abstracts, vol 10, pp EGU2008–A

Förste C, Bruinsma S, Abrikosov O, Lemoine J, Marty J, Flechtner F, Balmino G, Barthelmes F, Biancale RE (2015a) EIGEN-6C4 The latest combined global gravity field model including GOCE data up to degree and order 2190 of GFZ Potsdam and GRGS Toulouse. GFZ data services. http://doiorg/105880/icgem20151

Förste C, Bruinsma S, Rudenko S, Abrikosov O, Lemoine JM, Marty JC, Neumayer H, Biancale R (2015b) EIGEN-6S4: a time-variable satellite-only gravity field model to d/o 300 based on LAGEOS, GRACE and GOCE data from the collaboration of GFZ Potsdam and GRGS Toulouse. In: EGU general assembly conference abstracts, vol 17, p 3608

Fuchs MJ, Bouman J (2011) Rotation of GOCE gravity gradients to local frames. Geophys J Int 187(2):743–753

Gropp W, Lusk E, Skjellum A (1999) Using MPI: portable parallel programming with the message-passing interface, vol 1. MIT Press, Cambridge

Gruber T, Rummel R, Abrikosov O, van Hees R (2010) GOCE level 2 product data handbook. Technical report, GO-MA-HPF-GS-0110

Heiskanen WA, Moritz H (1967) Physical geodesy. Bull Géod 86(1):491–492

Holota P (1989) Boundary value problems and invariants of the gravitational tensor in satellite gradiometry. In: Theory of satellite geodesy and gravity field determination, Springer, pp 447–457

Ihde J, Adam J, Gurtner W, Harsson B, Sacher M, Schlüter W, Wöppelmann G (2002) The height solution of the European vertical reference network (EUVN), Mitteilungen des BKG, Bd. 25, EUREF Publication No. 11/I, Frankfurt a. M, Germany pp 53–79

Klees R, Koop R, Visser P, Van den Ijssel J (2000) Efficient gravity field recovery from GOCE gravity gradient observations. J Geod 74(7–8):561–571

Knudsen P, Benveniste J (2011) GOCE user toolbox and tutorial. In: Proceedings of the 4th international GOCE user workshop, European Space Agency, ESA Publication SP-696, 4p Munich

Knudsen P, Bingham R, Andersen O, Rio MH (2011) A global mean dynamic topography and ocean circulation estimation using a preliminary GOCE gravity model. J Geod 85(11):861–879

Koop R (1993) Globel gravity field modeling using satellite gravity gradiometry. Publications on Geodesy, vol 38

Li J, Jiang W, Zou X, Xu X, Shen W (2014) Evaluation of recent GRACE and GOCE satellite gravity models and combined models using GPS/leveling and gravity data in china. In: Gravity, geoid and height systems, Springer, pp 67–74

Mayrhofer R, Pail R, Fecher T (2010) Quick-look gravity field solution as part of the GOCE quality assessment. In: Proceedings of the ESA living planet symposium, vol 28

Metzler B, Pail R (2005) GOCE data processing: the spherical cap regularization approach. Stud Geophys Geod 49(4):441–462

Migliaccio F, Reguzzoni M, Sansò F (2004) Space-wise approach to satellite gravity field determination in the presence of coloured noise. J Geod 78(4–5):304–313
Migliaccio F, Reguzzoni M, Gatti A, Sansò F, Herceg M (2011) A GOCE-only global gravity field model by the space-wise approach. In: 4th international GOCE user workshop
Milbert DG (1998) Documentation for the GPS benchmark data set of 23-July-98. IGES Bull 8:29–42
Pacheco PS (1997) Parallel programming with MPI. Morgan Kaufmann, Burlington
Pail R, Plank G (2002) Assessment of three numerical solution strategies for gravity field recovery from GOCE satellite gravity gradiometry implemented on a parallel platform. J Geod 76(8):462–474
Pail R, Schuh WD, Wermuth M (2005) GOCE gravity field processing. In: Gravity, geoid and space missions, Springer, pp 36–41
Pail R, Bruinsma S, Migliaccio F, Förste C, Goiginger H, Schuh WD, Höck E, Reguzzoni M, Brockmann JM, Abrikosov O, Martin V, Thomas F, Reinhard M, Ina K, Fernando S, Carl CT (2011) First GOCE gravity field models derived by three different approaches. J Geod 85(11):819–843
Pavlis NK, Holmes SA, Kenyon SC, Factor JK (2012) The development and evaluation of the Earth Gravitational Model 2008 (EGM2008). J Geophys Res Solid Earth 117(B4)
Rapp RH (1973) Improved models for potential coefficients and anomaly degree variances. J Geophys Res 78(17):3497–3500
Reguzzoni M, Tselfes N (2009) Optimal multi-step collocation: application to the space-wise approach for GOCE data analysis. J Geod 83(1):13–29
Reigber C (1989) Gravity field recovery from satellite tracking data. In: Theory of satellite geodesy and gravity field determination, Springer, pp 197–234
Rummel R (1993) On the principles and prospects of gravity field determination by satellite methods. In: Geodesy and physics of the earth, Springer, pp 67–70
Rummel R, Colombo O (1985) Gravity field determination from satellite gradiometry. Bull Géod 59(3):233–246
Rummel R, Yi W, Stummer C (2011) GOCE gravitational gradiometry. J Geod 85(11):777–790
Sacerdote F, Sansò F (1989) Some problems related to satellite gradiometry. Bull Géod 63(4):405–415
Schuh WD (1996) Tailored numerical solution strategies for the global determination of the Earth's gravity field. Mitteilungen der geodtischen Institute der Technischen Universitt Graz, Folge 81, Graz
Schuh WD (2003) The processing of band-limited measurements; filtering techniques in the least squares context and in the presence of data gaps. In: Earth gravity field from space from sensors to earth sciences, Springer, pp 67–78
Taylor B (1717) Methodus incrementorum directa & inversa. Inny
Teunissen PJ (2000) Adjustment theory: an introduction. Delft University Press, Delft
Vermeer M (1990) Observable quantities in satellite gradiometry. Bull Géod 64(4):347–361
Wan XY, Yu JH, Zeng YY (2012) Frequency analysis and filtering processing of gravity gradient data from GOCE. Chin J Geophys 55(5):530–538
Yi W (2012) An alternative computation of a gravity field model from GOCE. Adv Space Res 50(3):371–384
Yu J, Zhao D (2010) The gravitational gradient tensors invariants and the related boundary conditions. Sci China Earth Sci 53(5):781–790
Yu J, Wan X (2013) Recovery of the gravity field from GOCE data by using the invariants of gradient tensor. Sci China Earth Sci 56(7):1193–1199
Zhang C, Guo C, Chen J, Zhang L, Wang B (2009) EGM2008 and its application analysis in Chinese Mainland. Acta Geod Cartogr Sin 38(4):283–289

Publisher's Note Springer Nature remains neutral with regard to jurisdictional claims in published maps and institutional affiliations.

Affiliations

Biao Lu[1,2,3] · Zhicai Luo[4,5] · Bo Zhong[1,6] · Hao Zhou[4] · Frank Flechtner[2,3] · Christoph Förste[2] · Franz Barthelmes[2] · Rui Zhou[7]

Biao Lu
biaolu@gfz-potsdam.de

Zhicai Luo
zcluo@hust.edu.cn

Hao Zhou
zhouh@hust.edu.cn

Frank Flechtner
flechtne@gfz-potsdam.de

Christoph Förste
foer@gfz-potsdam.de

Franz Barthelmes
bar@gfz-potsdam.de

Rui Zhou
einsteino@126.com

[1] School of Geodesy and Geomatics, Wuhan University, Wuhan 430079, People's Republic of China

[2] GFZ German Research Centre for Geosciences, Telegrafenberg, 14473 Potsdam, Germany

[3] Department of Geodesy and Geoinformation Science, Technical University of Berlin, 10623 Berlin, Germany

[4] MOE Key Laboratory of Fundamental Physical Quantities Measurement, School of Physics, Huazhong University of Science and Technology, Wuhan 430074, People's Republic of China

[5] Institute of Geophysics, Huazhong University of Science and Technology, Wuhan 430074, People's Republic of China

[6] Key Laboratory of Geospace Environment and Geodesy, Ministry of Education, Wuhan University, Wuhan 430079, People's Republic of China

[7] Zhengzhou Information Engineering University, Zhengzhou 450052, People's Republic of China